Science of the Total Environment xxx (xxxx) 179430

Contents lists available at ScienceDirect

Science of the Total Environment

journal homepage: www.elsevier.com

Quantification of SO_2 and CO_2 emission rates from coal-fired power plants in the Korean peninsula via airborne measurements

Jeonghwan Kim [a], Gangwoong Lee [a], Jongbyeok Jun [a], Beom-Keun Seo [a, b], Yongjoo Choi [a, *]

[a] Department of Environmental Science, Hankuk University of Foreign Studies, Yongin, South Korea
[b] Environmental Research Center, Hanseo University, Seosan, South Korea

HIGHLIGHTS

- Developed an ensemble model to quantify SO_2 and CO_2 emissions using top-down methods.
- Validated model with strong SO_2 correlations to CleanSYS monitoring system.
- Increased in CO_2 with decreasing SO_2 emission despite stable electricity production.
- Demonstrated the application of ensemble method for regulatory compliance.

GRAPHICAL ABSTRACT

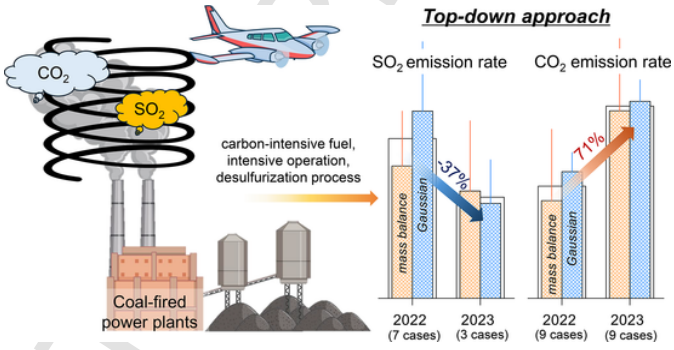

ARTICLE INFO

Editor: Hai Guo

Keywords:
Emission rates
Mass balance
Gaussian footprint
Coal-fired power plants
Airborne measurement

ABSTRACT

A reliable ensemble averaging method was developed to quantify sulfur dioxide (SO_2) and carbon dioxide (CO_2) emission rates from the Taean and Dangjin power plants in South Korea. This method integrated mass balance and Gaussian footprint approaches while accounting for individual uncertainties and deviations arising from distinct modeling assumptions and measurement variability. Eighteen representative spiral flights in 2022 (9 cases) and 2023 (9 cases) were conducted to evaluate emission rates and revealed several optimal conditions for achieving accurate quantification, including a small spiral radius with a fine vertical resolution under unstable atmospheric conditions. Validation of the estimated SO_2 emission rate revealed comparable correlation coefficients ($R > 0.72$) between the two methods and the real time automatic telemonitoring system (CleanSYS). The ensemble averaging method mitigated the sensitivity of the Gaussian footprint to the effects of meteorological conditions and high uncertainty in the mass balance, which resulted in an improved correlation of the estimated SO_2 emission rate with that measured by the CleanSYS ($R > 0.78$). When the same approach was applied, the CO_2 emission estimates from both methods showed a high correlation ($R > 0.78$) and confirmed the robustness of our ensemble averaging method. Although there was no significant difference between monthly electricity production in 2022 (October and November) and 2023 (May, October and November), the SO_2 emission rates decreased by 37 % and 29 % compared with the ensemble averaging method and CleanSYS, respectively; however, CO_2 emission rates increased by approximately 62 % at Taean and 83 % at Dangjin. This could be attributed to the use of carbon-intensive fuel sources, more intensive operations during research flight, and the desulfurization process, which aimed to reduce SO_2 emissions and release CO_2 as a byproduct. This study highlights the broad

* Corresponding author.
E-mail address: choingjoo@hufs.ac.kr (Y. Choi).

https://doi.org/10.1016/j.scitotenv.2025.179430
Received 12 December 2024; Received in revised form 15 March 2025; Accepted 11 April 2025
0048-9697/

application of our ensemble averaging method for emission monitoring and regulatory compliance, particularly for CO2, when real-time emission monitoring systems are absent.

1. Introduction

Coal-fired power plants are major contributors to atmospheric pollution, releasing significant quantities of sulfur dioxide (SO_2) and carbon dioxide (CO_2) (Grant et al., 2021; Kim et al., 2023). SO_2 is a key precursor to acid rain, severely impacts ecosystems, degrades water quality, and poses significant health risks through respiratory issues (Cape et al., 2003; Orellano et al., 2021). CO_2, which accounts for 88.5 % of total greenhouse gas emissions in South Korea (Jeon et al., 2010), is the main contributor to global warming and the associated climate impacts. According to the Clean Air Policy Support System (CAPSS) inventory in Korea (Choi et al., 2020), 81 % of the emitted SO_2 is attributed to point sources, especially coal-fired power plants, accounting for 31 % of these emissions. Additionally, coal combustion produces significantly more CO_2 per unit of heat energy than other fossil fuels do, making coal a major contributor to greenhouse gas emissions (Jeon et al., 2010). Prior to May 2017, the energy policy in South Korea included expanded coal-fired power generation, contributing to nearly 50 % of energy production due to its cost-effectiveness compared with other energy sources (Park et al., 2023). In response to the growing concerns about global warming, the Korean government implemented the 9th Basic Plan for Power Demand and Supply (2020–2030) to reduce CO_2 emissions by 28.5 % and decommission 56 coal-fired power plants by 2030. However, as demands for global energy have increased and coal continues to be a key energy source, the management of emissions from coal-fired power plants is vital for improving air quality and implementing climate change mitigation strategies (Cassia et al., 2018; Köne and Büke, 2010; Szulejko et al., 2017).

Bottom-up approaches, with estimates based on reported activities and emission factors, are often limited by inaccurate identification of emission sources and neglect the consideration of time-dependent fluctuations (Elguindi et al., 2020; Kurokawa et al., 2013; McDuffie et al., 2020; Qu et al., 2022). These methods are frequently hindered by uncertainties in both activity and emission factor data, which leads to potential discrepancies of up to 30 to 40 % in China (Qu et al., 2022) and 15 to 30 % in South Korea (Wong et al., 2024a), in emission inventories compared with in-situ measurements and/or top-down atmospheric estimates. As a result, top-down methodologies, which are based on measurements to estimate emission rates, have become comprehensive methods for the validation of targeted emission sources and estimate improvements.

Satellites have been extensively utilized in previous studies to monitor air quality and estimate emissions due to their broad spatial coverage and ability to detect large-scale emission patterns over extended periods at regional to global scales (Carn et al., 2007; Davis et al., 2019; Duncan et al., 2014; Frins et al., 2011; Kuhlmann et al., 2021; McLinden et al., 2012; Qu et al., 2022; Sanchez et al., 2019; Theys et al., 2015). However, despite these advantages, emission rates from satellite observations face notable limitations that affect their accuracy and applicability for certain emission sources, struggle to capture short-term (hourly to daily) variations in emission rates, and may be limited by spatial resolution and cloud cover. Open-path remote sensing is less effective for modeling elevated emissions from high-level point sources, such as stacks at coal-fired power plants, due to geometric and line-of-sight constraints. Although airborne observations can be costly and resource intensive to obtain, they can provide a distinct advantage for accurately quantifying emissions, particularly from large point sources (e.g., power plants and livestock). In addition, airborne measurements provide real-time information that can capture the high spatial and temporal variability of emissions with high precision by overcoming the limitations of satellite observations (Cambaliza et al., 2014; Fiehn et al., 2020; Gordon et al., 2015). This airborne approach is particularly valuable in monitoring emissions from small-scale facilities or detecting unreported sources in areas where real time automatic telemonitoring systems (CleanSYS), which are typically installed only at large-scale industrial sites, are unavailable.

In this context, previous studies have shown that top-down methodologies can be used to validate or improve current emission inventories, which enables more accurate environmental monitoring, enhances our understanding of emission patterns, allows progress toward emission reduction goals, and facilitates the development of mitigation strategies (Table 1). The mass balance and Gaussian footprint approaches are essential methods among the top-down approaches. The mass balance method is widely used for estimating reasonable emission rates for various pollutants (SO_2, CO_2, CH_4, CO, and NO_x) from various emission sources, such as oil sand production (Gordon et al., 2015), coal mining and industrial activities (Fiehn et al., 2020), oil and gas facilities (Fried et al., 2020), and power plants (Wong et al., 2024b). Although the accuracy of the mass balance method is highly sensitive to meteorological conditions and influenced by the spatial coverage and the resolution of measurements, it can be effectively utilized in various applications when certain measurement conditions are satisfied due to its inherently simple and practical methods. In addition, the Gaussian footprint approach can provide realistic results in cases with localized sources (refineries, ships, power plants, and urban industrial sources) and can be used to identify spatial emission patterns and the interannual variability of pollutant sources (Brioude et al., 2011). Gaussian models are particularly useful for simulating complex source locations and dispersion dynamics but are sensitive to uncertainties in input parameters (Mao et al., 2022). To leverage the advantages of both approaches, the ensemble averaging method (hereafter, ensemble method) not only mitigates biases inherent in individual methods but also provides a comprehensive assessment of uncertainty due to different modeling assumptions.

With the goal of developing a top-down ensemble method for comprehensive assessments of emission rates with high precision, a key aspect of this study is the validation of SO_2 and CO_2 emission rates from coal-fired power plants in bottom-up emission inventories, for which CO_2 is not a target species in the CleanSYS system. Hence, to ensure the robustness of the mass balance and Gaussian footprint approaches proposed by Kim et al. (2023), the estimated SO_2 emission rates were validated by comparison with CleanSYS data. Consequently, the same validation approach was applied to estimate CO_2 emission rates and leveraged a cross-validation process. Finally, by investigating the differences in the estimated SO_2 and CO_2 emission rates from eighteen cases between 2022 and 2023, we verified the accuracy of the bottom-up emission inventories and analyzed the causes of different trends in the SO_2 and CO_2 emission rates. This study not only provides accurate SO_2 and CO_2 emission estimates from power plants but also contributes to the broader field of atmospheric science by demonstrating the efficacy of two top-down methodologies for improving emission inventories.

2. Materials and methods

2.1. Coal-fired power plants in the study area

This study focuses on emission rates from the Taean (36.90° N, 126.24° E) and Dangjin (37.06° N, 126.51° E) coal-fired power plants, which are located approximately 30 km apart in the western coastal region of Taean, South Korea (Fig. 1). Given that these power plants are located in coastal regions, stack plumes are frequently observable over background marine concentrations, particularly under daytime seabreeze conditions (Chang et al., 2022; Geddes et al., 2021; Souri et al.,

Table 1
Comparisons between top-down and bottom-up methods conducted in various studies.

Gas	Study area	Method	Bottom-up inventory	Comparison with bottom-up	Reference
CH_4	Northwest Europe	Inverse model	UNFCCC[a], EDGAR[b]v4.0	Top-down inverse modeling results from 2001 to 2006 were 40 % and 21 % higher than UNFCCC and EDGARv4.0, respectively.	(Bergamaschi et al., 2010)
NO_x, CO, CO_2	Los Angeles, USA; South Coast Air Basin (SoCAB)	Mass balance, Inverse model	NEI[c] 2005, Vulcan 2002 and 2005, CARB[d] 2008	CO and NOx posterior estimates were 43 %, 32 % lower for LA and 37 % and 27 % lower for SoCAB compared to NEI 2005. CO was 15 % higher compared to CARB 2008. CO_2 posterior estimates were 31–44 % and 15–38 % higher in LA and SoCAB compared to Vulcan 2002 and 2005	(Brioude et al., 2013)
CO_2	Indianapolis, USA	Mass balance	EPA CEMS[e]	Estimated results were overestimated but within the EPA uncertainty (29 %). One case was 60 % underestimated due to under-sampling	(Cambaliza et al., 2014)
CO_2	Baltimore-Washington, USA	Mass balance	EDGARv4.3.2, ACES[f]v1, FFDAS[g]v2.2, ODIAC[h]2018	All bottom-up inventories for fossil fuel CO_2 emissions were 15 % overestimated	(Ahn et al., 2020)
NO_x, SO_2, CO	China, India	Inverse model	HTAP[i]v2	Estimated NO_x emission rates were 21–26 % and 28 % lower in China and India. SO_2 estimates were within 4 % difference in China but 39–61 % lower in India. Top-down CO estimates were 43–62 % and 25–38 % higher in China and India.	(Qu et al., 2022)
CH4	Global	Inversion model	CEDS[j], EDGARv4.3.2, GAINS ECLIPSE[k]v6, US EPA[l] 2012, FAO[m], FINN[o]v1.5, GFAS[p]v1.3, GFED[q]v4.1s, QFED[r]v2.4r1	Median bottom-up estimate value from 2008 to 2017 were 136 Tg yr^{-1} higher than median top-down estimate value for total CH_4 emission rates	(Hajny et al., 2023)
SO_2	Taean, South Korea	Mass balance, Inverse model	CAPSS[s] 2017, TMS[t]	SO_2 emission rates estimated by mass balance and inverse method were 51 % and 90 % of TMS data and 58 % and 101 % of CAPSS 2017, respectively.	(Kim et al., 2023)
SO_2, CO_2	Taean, South Korea	Mass balance	CAPSS 2018, TMS	Mass balance estimates of SO_2 were 85 % and 129 % of TMS at Dangjin and Taean power plants. Dangjin, Taean, Hyundai, and Daesan estimates were 38 %, 60 %, 40 %, and 67 % underestimated of the reported CAPSS 2018 emission rates, respectively.	(Wong et al., 2024a)

[a] UNFCCC: United Nations Framework Convention on Climate Change.
[b] EDGAR: Emissions Database for Global Atmospheric Research.
[c] NEI: National Emission Inventory.
[d] CARB: California Air Resources Board.
[e] CEMS: Continuous Emission Monitoring System.
[f] ACES: Anthropogenic Carbon Emission System.
[g] FFDAS: Fossil Fuel Data Assimilation System.
[h] ODIAC: Open Data Inventory for Anthropogenic Cabon dioxide.
[i] HTAP: Hemispheric Transport of Air Pollution.
[j] CEDS: Community Emissions Data System.
[k] GAINS ECLIPSE: Greenhouse Gas and Air pollution Interactions and Synergies Evaluating the Climate and Air Quality Impacts of Short-Lived Pollutants.
[l] EPA: Environmental Protection Agency.
[m] FAO: Food and Agriculture Organization.
[o] FINN: Fire Inventory.
[p] GFAS: Global Fire Assimilation System.
[q] GFED: Global Fire Emissions Database.
[s] CAPSS: Clean Air Policy Support System.
[t] TMS: Tele-Monitoring System.
[u] QFED: Quick Fire Emissions Dataset

2023). The Taean and Dangjin power plants are among the largest coal-fired power plants in the world in terms of power generation capacity (6.1 GW yr^{-1} for Taean and 6.0 GW yr^{-1} for Dangjin), contributing significantly to pollutant emissions (Grant et al., 2021; Nassar et al., 2021). The Taean power plant consists of ten power units with 150 m stack heights, which emit a total of 3.50 Gg of SO_2 according to CAPSS 2021 and approximately 25.8 Tg of CO_2 according to the Emission Database for Global Atmospheric Research (EDGAR; Crippa et al., 2023) v8.0 in 2022. Similarly, the Dangjin power plant features eight power units with 150 m stacks and two power units with 208 m stacks,

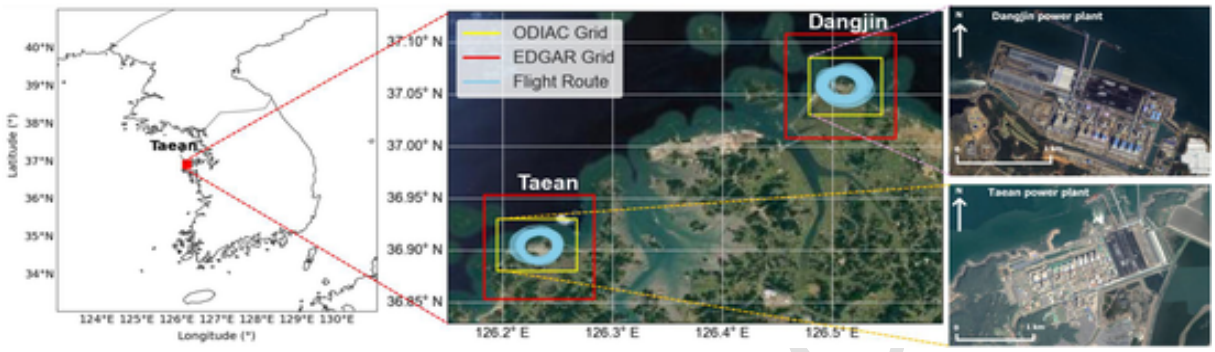

Fig. 1. Geolocation of Taean (36.90˚ N, 126.24˚ E) and Dangjin (37.06˚N, 126.51˚E) coal-fired power plants in the western coastal region of South Korea. Taean and Dangjin power plants are approximately 1.5 km^2 and 1.8 km^2 in area, respectively. Comparison of the grid size used for ODIAC (yellow box) and EDGAR (red box) emission inventory with all flight routes (sky blue lines) conducted in this study. The images were obtained from Google Earth.

which emitted a total of 4.05 Gg of SO_2 according to CAPSS 2021 and 27.5 Tg of CO_2 according to EDGARv8.0 in 2022. Notably, the emission conditions (e.g., exit gas temperature, exit gas velocity, stack height, and stack diameter) for each stack are continuously monitored in real time via CleanSYS. According to the national standard for stack monitoring, the uncertainty in SO_2 emission measurements must be kept below 20 % relative to the daily emission limit value (ELV) of 48 ppm. We assumed a 20 % relative error in the CleanSYS emission rates. This assumption was based on the uncertainties observed in CleanSYS SO_2 measurements, where the errors compared with the ELV ranged from 3.5 % to 5.4 %, and the percentage errors relative to the reference methods varied from 8.9 % to 21 % (Kim et al., 2023).

2.2. Airborne measurements

Airborne measurements were conducted via a modified Beechcraft KingAir-C90GT aircraft (Seo et al., 2019) equipped with advanced instrumentation for the real-time monitoring of SO_2 and CO_2 concentrations. SO_2 was measured using the 43iQTL analyzer (Thermo Scientific, USA), which provides high sensitivity (0.2 ppb) and a rapid response (<10 s), whereas CO_2 concentrations were monitored with the Off-Axis Integrated Cavity Output Spectroscopy (OA-ICOS; LGR GLA331-MCEA1, Los Gatos Research, Inc., USA) analyzer, which is known for its high response time (<10 s with an external pump) and precision (1σ, 1 s: ±0.2 ppm). Both instruments operate at a high temporal resolution of 1 Hz, enabling the capture of the spatial variability of emissions.

In conjunction with the gas analyzers, the AIMMS-30 (Aircraft Integrated Meteorological Measurement System; Aventech Research, Inc., Canada) system was employed to collect detailed meteorological data for interpreting data from airborne observations. The AIMMS-30 is a comprehensive airborne meteorological system that integrates multiple sensors to measure wind vectors (*U*, *V*, *W*), temperature, humidity, and pressure, which are particularly important for understanding plume dispersion. The accuracies of the meteorological parameters are ±0.4 m s^{-1} for wind speed, ±2˚ for wind direction, ±0.3 ˚C for temperature, and ± 2 % for humidity. The pressure sensor provides an accuracy of ±0.1 hPa, with pressure an important parameter for determining altitude and understanding atmospheric layering. The AIMMS-30 system provides these data at a 1 Hz frequency, ensuring synchronization with the gas analyzers; thus, a high-resolution temporal characterization of the pollution plume can be obtained to perform comprehensive and detailed assessments of emission dynamics.

2.3. Mass balance approach

The mass balance method evaluates emissions by considering the inflow and outflow of mass through the boundaries of a defined box that surrounds the emission sources. This method assumes that the net flux originates entirely from within the enclosed box. To estimate the mass flux, horizontal fluxes at all grid points, with a vertical resolution of 9.5 m along the z-axis and 140 m along the y-axis, are projected onto a two-dimensional plane for each flight. A kriging algorithm is applied to interpolate the observed concentrations between downwind transects of the trace gas plume, enabling mass flux calculations through this plane. The differences between the mean influx and outflux are then computed to derive the emission rates for the stack sources within the box.

Given the high elevations of stack emission plumes, linear extrapolation was employed to estimate SO_2 and CO_2 concentrations from the lowest airborne observation altitudes (~400 m) to the ground level. For SO_2, the minimum concentration for each spiral was assumed to be at ground level, whereas for CO_2, background levels were determined via the lowest one percentile of airborne observations for each flight. Notably, the effect of differences in percentiles might be negligible because significant differences in estimated emission rates between two different background concentrations were not observed (<10 %). These background concentrations were then linearly extrapolated from the ground to the lowest airborne measurements, allowing for an accurate calculation of the flux within the control volume. A key advantage of the mass balance method is that it does not require prior values or external input parameters, such as stack characteristics or detailed meteorological data. This flexibility makes it highly suitable for estimating emission rates directly from observational data. In this study, we applied a modified version of the top-down mass balance method proposed by Kim et al. (2023), which enhances the ability to capture emissions with minimal dependency on external parameters.

The uncertainty in the mass balance approach was rigorously calculated by considering the potential errors associated with each input variable, including gas concentration (12 % relative uncertainty), wind speed (0.4 m s^{-1} absolute uncertainty based on device specifications), and the angle of attack (θ) with an absolute uncertainty of 0.04. The combined uncertainty was evaluated with the propagation of uncertainty method.

2.4. Gaussian footprint approach

The inverse Gaussian footprint method allows for the calculation of emission sensitivity by establishing the relationship between emission rates (g s^{-1}) at receptor points and pollutant concentrations (ppbv) at source locations, as outlined by Seibert and Frank (2004) and Stohl et al. (2009). This approach generates SO_2 and CO_2 footprint fields (ppbv s g^{-1}) via a backward Gaussian plume model, where inverted wind data from specific sampling locations serve as the initial wind field. To accurately simulate model dispersion, both horizontal and vertical disper-

sion coefficients were derived as functions of downwind distance, accounting for variations across different atmospheric stability classes. These stability classes were determined on the basis of solar radiation and wind speed measurements during the sampling period (Table 2) and using the Pasquill classification scheme (Kahl and Chapman, 2018). The effective stack height, which was calculated using the Pasquill classification and the Briggs equation (Briggs, 1969) and considering buoyancy and momentum effects, was used as the starting point for plume dispersion in the Gaussian model.

The Bayesian regression framework used in this study, with monthly emission rates of SO_2 from CAPSS 2021 and CO_2 from EDGARv8.0 as prior inputs, was implemented through the Just Another Gibbs Sampler (JAGS) package in R (v.4.4.1), and this approach provides a robust method for estimating regression coefficients and quantifying their uncertainties. The priors are designed to reflect minimal prior assumptions while ensuring numerical stability during estimation. Using Markov Chain Monte Carlo (MCMC) sampling through the JAGS package, posterior distributions are generated for all parameters and offer a probabilistic representation of their likely values. The uncertainty in the Gaussian footprint approach is assessed through posterior summaries and includes mean estimates (central tendency), standard deviations (variability), and 95 % confidence intervals.

Additional data, such as meteorological conditions and stack-specific parameters, are essential for estimating emissions at observation points to accurately estimate concentrations from stacks. Tables S1 and S2 summarize the conditions of the seven stacks associated with the ten power units at both the Taean and Dangjin power plants. All the stacks had heights of approximately 150 m, with diameters ranging from 5.4 to 7.7 m. The gas exit velocities and temperatures were continuously monitored by the real-time CleanSYS system, with the exit temperatures from all the stacks approximately 50 ˚C higher than the surrounding ambient air.

In this study, we used the overall mean values as input parameters regardless of the stack number and measurement date instead of the hourly measured gas exit velocity and temperature for each stack. Because the differences between the two approaches could be neglected within <1 % for SO_2 and 0.9 % for CO_2, the use of the average gas exit velocity and temperature values can produce reliable estimates, although the Gaussian footprint model is well known to be sensitive to input parameters (Brioude et al., 2013; Kim et al., 2023; Mao et al., 2022). Thus, this approach could provide a solution when it is difficult to obtain detailed information for all stacks on specific research flight days.

Table 2
Summary of meteorological conditions and stability class for each spiral. The uncertainty associated with each estimate is indicated by the ± symbol, reflecting the quantified uncertainty bounds.

Date	Spiral	Location	Wind speed (m s^{-1})		Solar radiation (MJ m^{-2})	Stability class
			450 m	Ground level		
2022-10-12	S1T	Taean	4.86 ± 0.60	3.12 ± 0.61	1.76 ± 0.51	C
	S1D	Dangjin	4.38 ± 0.35	3.12 ± 0.61	1.76 ± 0.51	B
2022-10-21	S2D	Dangjin	4.41 ± 1.00	2.85 ± 0.60	1.60 ± 0.36	B
2022-10-25	S2T	Taean	4.41 ± 0.77	3.83 ± 0.95	2.07 ± 0.69	C
	S3D	Dangjin	4.07 ± 1.04	4.35 ± 1.07	2.37 ± 0.73	B
2022-10-26	S4D	Dangjin	3.09 ± 1.15	0.78 ± 0.49	0.83 ± 0.44	C
	S5D	Dangjin	2.24 ± 0.82	1.61 ± 0.69	1.48 ± 0.60	B
2022-11-02	S3T	Taean	3.48 ± 0.91	0.23 ± 0.59	0.85 ± 0.45	C
	S4T	Taean	3.32 ± 1.12	2.16 ± 0.70	2.00 ± 0.67	C
2023-05-09	S5T	Taean	6.05 ± 0.92	3.33 ± 0.63	2.88 ± 0.72	C
2023-05-10	S6T	Taean	3.00 ± 0.32	0.95 ± 0.41	2.09 ± 0.64	B
	S6D	Dangjin	2.27 ± 0.78	0.84 ± 0.53	2.10 ± 0.63	B
2023-05-25	S7T	Taean	2.41 ± 0.95	1.63 ± 0.61	1.84 ± 0.75	B
	S7D	Dangjin	4.35 ± 0.74	1.21 ± 0.61	2.56 ± 0.74	B
2023-10-18	S8D	Dangjin	4.79 ± 0.74	3.56 ± 0.79	2.12 ± 0.62	B
	S9D	Dangjin	4.00 ± 0.99	3.56 ± 0.79	2.12 ± 0.64	B
2023-10-31	S10D	Dangjin	5.11 ± 1.18	4.57 ± 0.85	1.86 ± 0.48	D
2023-11-08	S8T	Taean	2.16 ± 0.63	1.73 ± 0.62	2.10 ± 0.51	B

2.5. Ensemble method

Both the mass balance and Gaussian footprint methods provide an estimate of emission rates, but each estimate is associated with distinct variability or error due to various uncertainties (e.g., instrument accuracy or sampling conditions) and differences in the modeling methods (e.g., assumptions regarding atmospheric dispersion). This study used the ensemble method by averaging emission estimates from the mass balance and Gaussian footprint methods without applying specific weighting factors. This approach was chosen to maintain consistency and avoid potential biases that could arise from each method. However, the uncertainty of the ensemble method ($u_{ensemble}$) was calculated to capture both individual uncertainties from each method and provide a comprehensive assessment of the overall reliability of the emission estimates via Eqs. (1) and (2).

$$u_{ensemble} = \sqrt{\frac{N_{mass}u_{mass}^2 + N_{Gaussian}u_{Gaussian}^2 + N_{mass}d_{mass}^2 + N_{Gaussian}d_{Gaussian}^2}{N_{mass} + N_{Gaussian}}} \quad (1)$$

$$\bar{x} = \frac{N_{mass}x_{mass} + N_{Gaussian}x_{Gaussian}}{N_{mass} + N_{Gaussian}} \quad (2)$$

where $u_{ensemble}$ represents the standard deviation of the ensemble predictions for emission rates considering the overall mean value ($\bar{x}$), which is calculated by considering uncertainties from both the mass balance (u_{mass}) and Gaussian footprint ($u_{Gaussian}$) methods with certain sample sizes (N_{mass} and $N_{Gaussian}$). d_{mass} and $d_{Gaussian}$ represent the deviations of each method from the overall mean value as $x_{mass} - \bar{x}$ and $x_{Gaussian} - \bar{x}$, respectively.

2.6. Meteorological conditions during research flights

Table 2 provides a summary of the meteorological conditions for eighteen selected spiral flights during the campaigns in 2022 and 2023. The ground-level wind speed and solar radiation data were obtained from the Seosan station (36.78° N, 126.49° E), which is the nearest Automated Synoptic Observing System (ASOS) station operated by the Korea Meteorological Administration (KMA). For the airborne observations in this study, the aircraft conducted circular flights around the power plant at 58 different altitudes ranging from approximately 400–1200 m above sea level. These altitudes were carefully selected to intercept SO_2 and CO_2 plumes within an approximately 2 km radius from the stacks to ensure that the plumes retained their distinct patterns considering background levels while remaining below the boundary layer. For safety reasons, flight operations were restricted to altitudes above 350 m.

On the basis of Table 2, the atmospheric stability on the flight days in 2022 and 2023 was predominantly classified as B or C, according to the Pasquill scheme, with only one flight day (S10D) classified as class D. These stability classes, indicative of moderate to slightly unstable atmospheric conditions, were characterized by moderate solar radiation and wind speed levels that facilitated daytime heating and intensified local wind. As a result, the wind speeds at 400 to 450 m were generally higher than those at ground level, although the vertical dispersion observed was less pronounced than what would be expected under more unstable class A conditions. Notably, the number of research flights for estimating emission rates for SO_2 (six for Taean and four for Dangjin)

was smaller than that for CO_2 (eight for Taean and ten for Dangjin) because of maintenance issues with the SO_2 instrument.

2.7. Bottom-up CO_2 emission inventories

In this study, we utilized the EDGAR emission inventory as the CO_2 prior dataset in the Gaussian footprint method. Specifically, we employed the EDGARv8.0 dataset, with a spatial resolution of 0.1° × 0.1° and as one of the most recently updated global emission inventories, providing monthly emissions data for 2022. EDGAR is widely recognized for its global coverage and accuracy, with country-specific emissions derived from international activity data and emission factors (Crippa et al., 2023). For comparison with our estimated CO_2 emission rates, we employed the Open-Source Data Inventory for Anthropogenic CO_2 (ODIAC) Fossil Fuel CO_2 emission dataset (Oda and Maksyutov, 2015; accessed: 2024/09/05) from 2022, which was initially developed as part of the Greenhouse Gases Observing Satellite (GOSAT) project in Japan. ODIAC offers a fine spatial resolution of 1 × 1 km, allowing for high-resolution spatial assessments of emissions and particularly suitable for analyzing emissions from localized point sources such as power plants. The spatial resolutions for both the EDGAR and ODIAC inventories, along with the flight routes used in this study, are displayed in Fig. 1. The uncertainty of both the EDGAR and ODIAC inventories was approximately 7.1 %, on the basis of global estimates from previous research (Oda and Maksyutov, 2011; Solazzo et al., 2021), which ensured consistency and robustness in comparing the emission rates derived from the Gaussian footprint method.

3. Results and discussion

3.1. Characteristics of the observed SO_2 and CO_2 plume structures

Spatially (vertical and horizontal) interpolated SO_2 and CO_2 concentrations for Dangjin (S10D) and Taean (S8T), along with the observed sampling points, are shown in Fig. 2. By applying the kriging method, curtain plots can provide clearer insights into plume heights and complex structures. A distinct plume core was observed at multiple transects at altitudes less than ~600 m for both SO_2 and CO_2. The SO_2 concentrations in S8T were approximately four times higher than those in S10D, indicating significant variability in the dispersion of SO_2 when considering the similar emission rates between the Taean and Dangjin power plants from CAPSS 2021 and CleanSYS (Table 3). The CO_2 concentrations exhibited a similar trend, with higher values also observed in S8T. Both flights were conducted in the afternoon, and the plumes were evenly distributed within the lower atmospheric layers, supporting the assumption of effective vertical mixing within the planetary boundary layer (PBL). These results emphasize that local meteorological conditions can influence the distribution and intensity of emissions for both SO_2 and CO_2. In addition, the SO_2 and CO_2 concentrations generally decreased along the background region over the Yellow Sea, where no dominant emission sources are located. However, increases in SO_2 and CO_2 concentrations were observed at lower altitudes that were distinct from the main plume. These notable upwind concentrations at low altitudes most likely came from sea level sources such as ships. Although the mass balance model accounted for and subtracted inflow within the sampling columns, elevated background concentrations may increase the uncertainty associated with emission rates estimated using top-down approaches.

Fig. 3 shows an example of footprint contours for sampling positions corresponding to the maximum SO_2 and CO_2 concentrations observed during S10D and S8T spirals. During the flights, the meteorological conditions played a significant role in dispersing the plume; notably, the difference in wind speed between S10D and S8T was high. The footprint for S8T at low wind speeds (2.16 m s^{-1} at 450 m and 1.73 m s^{-1} at ground level) was widely distributed but well-defined and aligned perpendicularly to the stacks, even under unstable conditions (Class B). In contrast, the footprint for S10D at high wind speeds (5.11 m s^{-1} at 450 m and 4.57 m s^{-1} at ground level) was dispersed with narrow isopleths, leading to a less evenly distributed footprint contour as the wind shifted northward. Consequently, the horizontal dispersion of plumes on S10D under stable conditions (class D) was more pronounced than the vertical dispersion. This reflects a general pattern of plume dispersion, where high wind speeds tended to flatten the plume, reducing vertical mixing and stretching the plume horizontally, whereas low wind

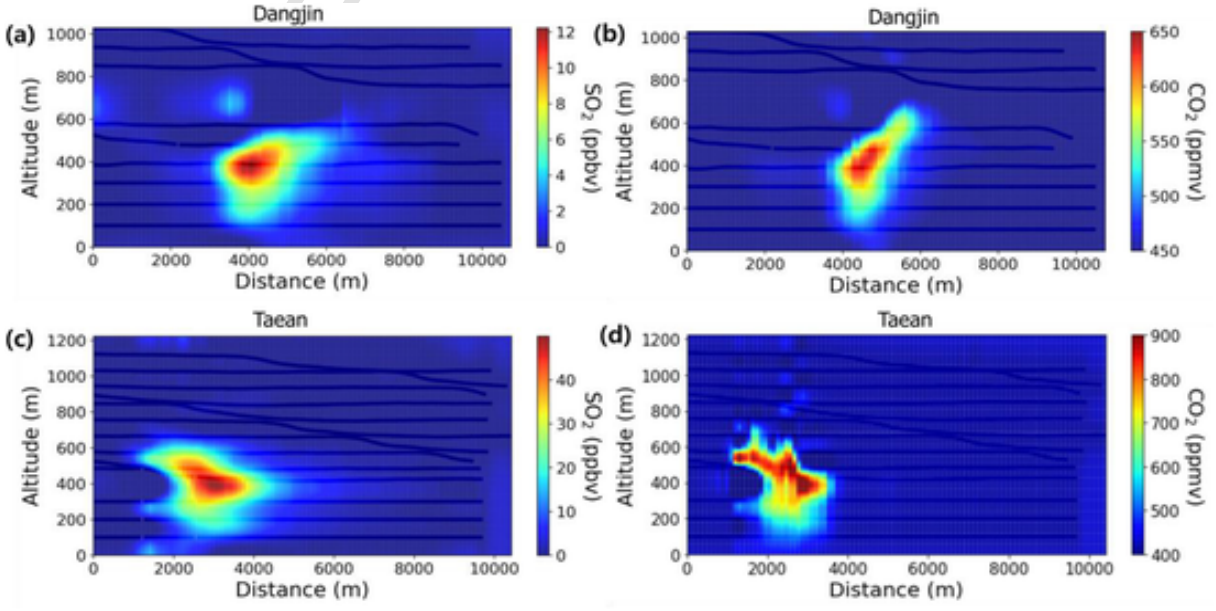

Fig. 2. Curtain plots of mass balance approach for Dangjin S10D (upper) and Taean S8T (lower). The plots (a) and (c) are SO_2, and plots (b) and (d) are CO_2. Concentrations between observation points were interpolated using the kriging method, and distances were calculated from the north end of flight tracks in an anticlockwise direction along the x-axis.

Table 3
Overall comparison of total emission rates of SO_2 (kg h^{-1}) for Taean and Dangjin powerplant implemented by the mass balance and Gaussian footprint methods. The uncertainty associated with each estimate is indicated by the ± symbol, reflecting the quantified uncertainty bounds. TMS and CAPSS emission inventory for each location included for comparison.

Location	Spiral	Mass balance	Gaussian footprint	Ensemble	TMS[a]	CAPSS 2021[b]
Taean	S1T	383 ± 232	404 ± 131	394 ± 189	490 ± 98	
	S2T	329 ± 117	394 ± 142	361 ± 134	351 ± 70	
	S3T	207 ± 91	341 ± 122	274 ± 127	386 ± 77	
	S4T	270 ± 87	337 ± 119	304 ± 110	386 ± 77	
	S5T	274 ± 239	240 ± 91	257 ± 181	362 ± 72	
	S8T	204 ± 112	232 ± 91	218 ± 103	250 ± 50	
	Mean	278 ± 146	325 ± 116	301 ± 141	371 ± 74	400 ± 116
Dangjin	S1D	161 ± 93	284 ± 124	222 ± 126	285 ± 57	
	S3D	193 ± 45	336 ± 130	264 ± 121	355 ± 71	
	S5D	231 ± 79	360 ± 132	296 ± 126	357 ± 71	
	S10D	160 ± 86	117 ± 71	139 ± 82	216 ± 43	
	Mean	186 ± 76	274 ± 114	230 ± 114	303 ± 61	462 ± 134

[a] TMS uncertainty: 20 % (Kim et al., 2023).
[b] CAPSS uncertainty: 29 % (Kim and Jang, 2014).

speeds tended to enhance vertical dispersion while reducing the horizontal distribution. These results emphasized that the Gaussian footprint method is somewhat unreliable under stable conditions, characterized by ineffective footprint identification and inaccurate emission rate estimation.

Therefore, we can summarize several important conditions for accurately quantifying emission rates, as follows. (1) Research flights should be conducted around fixed emission sources within a small radius to increase the possibility of observing plumes and minimize interference from other emission sources to ensure large differences from background concentrations. (2) Sampling altitudes less than the PBL height should be maintained to ensure comprehensive observations of the vertical distribution of the emitted plume. (3) Maintaining tight intervals between flight altitudes can enhance the vertical resolution of plume observations. Previous studies emphasized the importance of separating background concentrations from plume observations, and the number of flight transects at multiple altitudes is highly important for achieving accurate emission rate estimates (Cambaliza et al., 2014; Fiehn et al., 2020; Kim et al., 2023). (4) These strategies are essential for obtaining accurate and robust emission rates under optimal atmospheric sampling conditions with clear skies and low wind speeds as well as under unstable conditions to facilitate the detection of plume dispersion.

3.2. Comparison of the estimated emission rates for SO_2 with the CleanSYS

The estimated SO_2 emission rates for all the selected spirals calculated via both the mass balance and Gaussian approaches, as described in Section 3.1, are summarized in Table 3. The mass balance method demonstrated considerable variability in SO_2 emissions, with values of 278 kg h^{-1} ± 53 % at Taean and 186 kg h^{-1} ± 41 % at Dangjin. Similarly, the Gaussian footprint method provided more converged estimates of 325 kg h^{-1} ± 36 % at Taean and 274 kg h^{-1} ± 41 % at Dangjin. Considering the uncertainties in CAPSS (~29 %) (Kim and Jang, 2014) and CleanSYS (~20 %), the estimates obtained with the Gaussian footprint (>20 %) and mass balance method (>41 %) fall within an acceptable uncertainty range, but the Gaussian footprint approach displayed more stable performance than the mass balance method. This difference can be partially attributed to the extrapolation techniques employed in the mass balance method because the extrapolation relies on assumptions about vertical concentration gradients below the lowest measured altitude, which may not accurately reflect the actual plume behavior near the surface. Previous studies have also highlighted that the choice of extrapolation methods for extending airborne concentration data to ground level can significantly influence not only flux estimations but also the level of uncertainty (Gordon et al., 2015; Wong et al., 2024b). The correlations between the estimated SO_2 emission rates and real-time CleanSYS measurements converged within a narrow range with high correlation coefficients (R) of >0.72 for Taean and > 0.85 for Dangjin with the mass balance method (Fig. 4). While both approaches yielded acceptable ranges, slopes of the best-fit line were lower than unity, which indicated that the emission rates were underestimated compared with those of the CleanSYS, except for those obtained with the Gaussian method at Dangjin. For Taean, the slope of the best-fit line obtained with the Gaussian method (0.69) was slightly

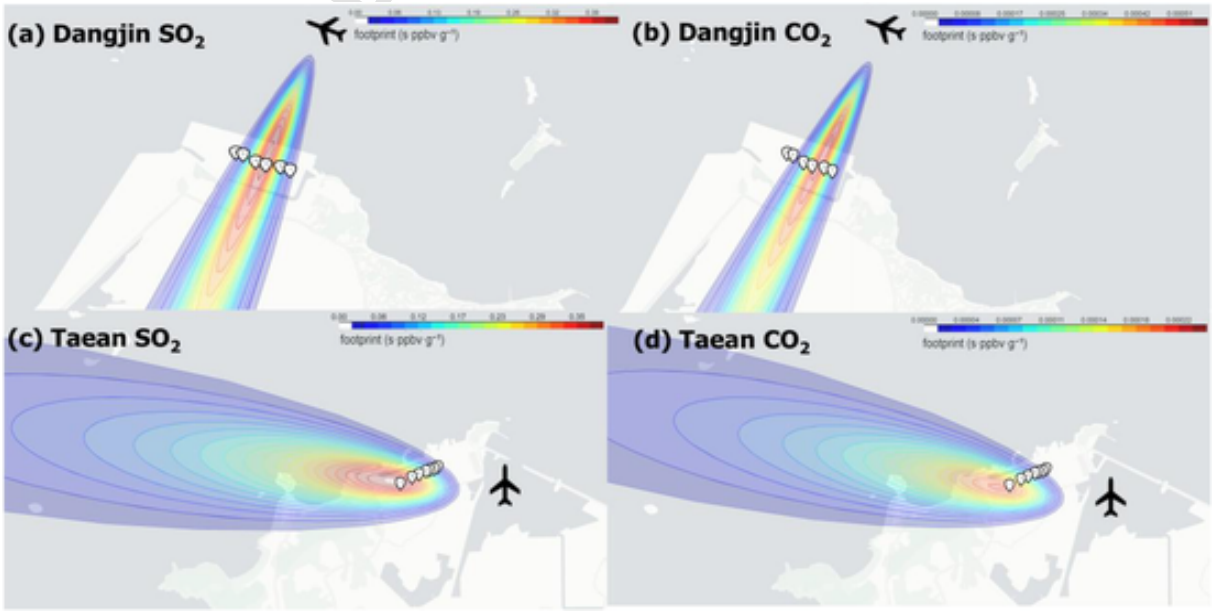

Fig. 3. Simulated Gaussian footprint results for Dangjin S10D (upper) and Taean S8T (lower). The plots (a) and (c) are SO_2, and plots (b) and (d) are CO_2.

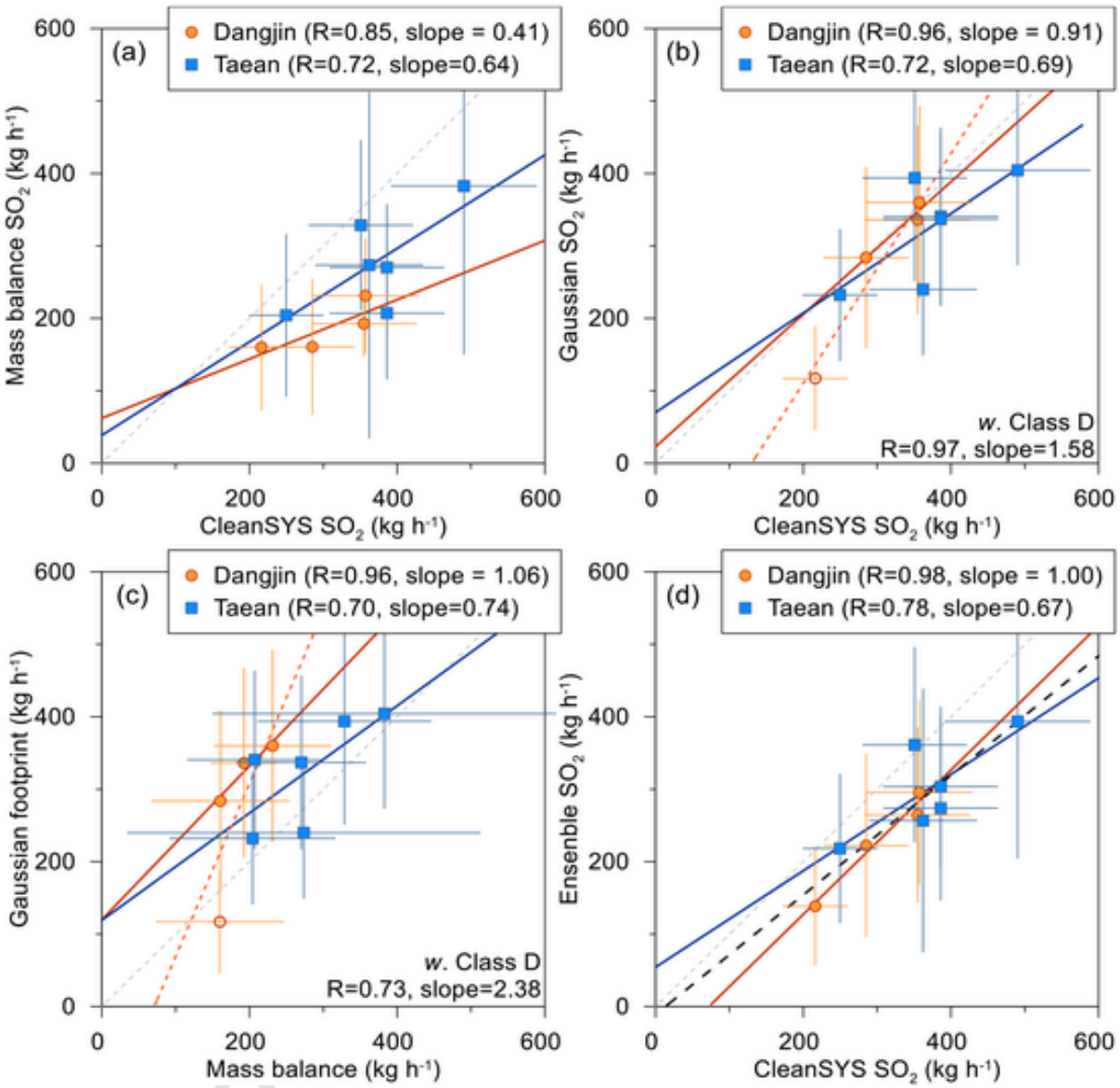

Fig. 4. The correlation between TMS and estimated results is displayed in Taean (a) and Dangjin (b) powerplant. Plots (c) and (d) indicate a comparison of the estimated SO_2 emission rates between mass balance and Gaussian footprint approaches and between TMS and our ensemble model, respectively. Open symbols in (b) and (c) represent data obtained under meteorological stability class D. The color solid lines (without Class D) and dashed lines (with Class D) indicate the best-fit line, while the gray dashed line represents the 1:1 line, respectively.

greater than that obtained with the mass balance approach (0.64), with a similar R of 0.72.

Whereas the Gaussian approach at Dangjin significantly overestimated the slope by 1.58 compared with the mass balance method (0.41), the slope obtained with the Gaussian approach decreased to 0.91 when the lowest emission rate on S10D under stable conditions (class D) with strong winds was excluded, as mentioned in Section 3.1. Similarly, the slope and R for the mass balance at Dangjin increased to 0.85 and 0.74, respectively, when class D was excluded, but the improvement in the correlation was much weaker than that in the Gaussian footprint. This result highlights that the estimated emission rates from both methods could be significantly influenced under stable conditions, especially in the Gaussian footprint approach for SO_2.

Although the estimated emission rates were slightly different depending on the approach used, the R values between the two methods were comparable, namely, 0.70 for Taean and 0.73 (0.96 without class D) for Dangjin (Fig. 4c), along with lower estimation rates for the mass balance method (Table 3). This might be attributed to the sparse vertical sampling resolution, particularly at low altitudes (< 400 m), resulting in a lack of representative information near the surface. Additionally, the large fluctuations in wind speed and direction during a research flight can decrease the accuracy of estimated emission rates due to inconsistent flux measurements because a steady-state plume is assumed in the mass balance method (Zondlo, 2021). Despite the limitations of the mass balance approach, its variation seems to be much narrower than that of the Gaussian footprint approach, which is sensitive under stable conditions at high wind speeds. This result suggests that averaging emission rates from the two approaches (the ensemble method) can provide reasonably estimated SO_2 emission rates by reducing the impact of inherent biases in each individual method. In other words, its flexibility in utilizing both direct observations (mass balance) and model-driven observations (the Gaussian footprint approach) makes it highly adaptable across diverse datasets and environmental conditions and enhances the reliability of the final results. Notably, the

R and slope of the best-fit line are improved, especially for Dangjin estimates (Fig. 4d).

However, the ensemble method also has limitations as its accuracy is inherently dependent on the quality of the input data, which means errors can propagate into the final estimates. Additionally, by averaging each estimation rate, some unique insights from individual methods may be diluted and potentially limit a more nuanced understanding of emission patterns. Despite these challenges, the ensemble method remains a valuable tool for achieving balanced and robust emission estimates when its limitations are carefully managed.

3.3. Estimation of CO_2 emission rates using the same approaches

Given that real-time CleanSYS installed on stacks at power plants do not monitor CO_2 emissions, there is no information on real-time CO_2 emission rates to validate our estimates directly. However, given the validated accuracy of SO_2 emission rates in Section 3.2, our ensemble method provides an alternative approach for accurately estimating CO_2 emissions when the same parameters that produce reliable SO_2 emission rates are applied. Considering the data used in the estimation of SO_2 emission rates, the quality of the estimated CO_2 emission rates was confirmed by similar R values (0.77 for Taean and 0.99 for Dangjin) and the slope of the best-fit line (0.52 for Taean and 1.15 for Dangjin) between the mass balance and Gaussian footprint methods (Fig. 5). For all the data, the R value between the mass balance and Gaussian footprint methods was high at >0.78 at both Taean and Dangjin, and the slope of the best fit lines was >0.48 for Taean and Dangjin. However, high intercepts ($\sim$1000 ton h^{-1}), which accounted for $\sim$50 % of the emission rates, indicated that mass balance might be overestimated at low emission rates, and vice versa.

The overall mean of the estimated emission rates from the mass balance approach was 1906 ton h^{-1} $\pm$ 51 % at Taean and 1775 ton h^{-1} $\pm$ 55 % at Dangjin (Table 4). The Gaussian footprint method yielded marginally higher average CO_2 emission rates at 2200 ton h^{-1} $\pm$ 12 % and 2007 ton h^{-1} $\pm$ 14 % for Taean and Dangjin, respectively; thus, the difference between these two methods was approximately 12 % at both power plants, which supports the accuracy of our ensemble method. In Dangjin, the difference increased to 22.5 % when accounting for the data used in the SO_2 calculations, suggesting that the difference was minimized as the number of available data points increased. Therefore, these results implied that both methods produced generally consistent emission estimates, demonstrating their robustness by compensating for their inherent limitations.

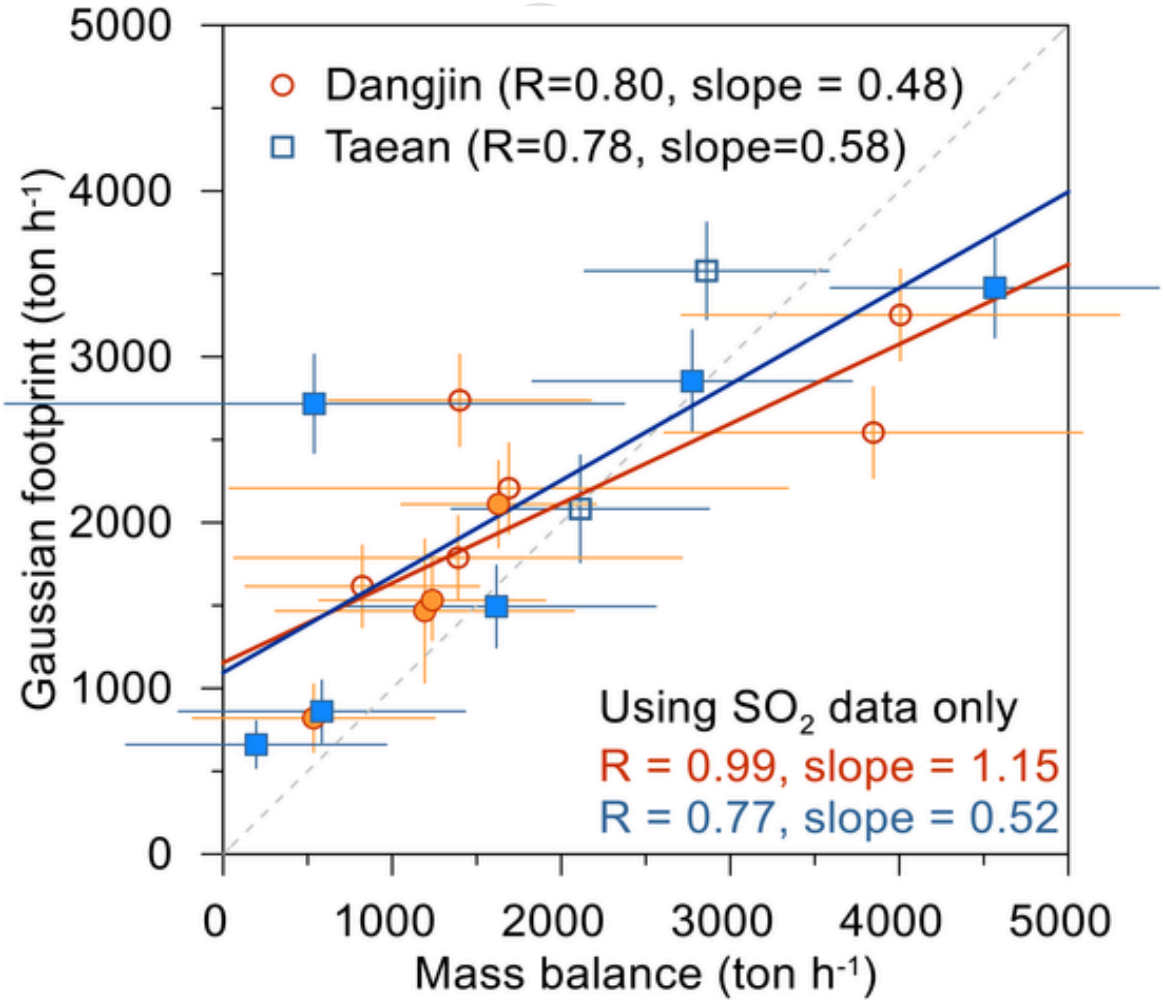

Fig. 5. Correlation of CO_2 estimated emission rates between mass balance and Gaussian footprint approaches at Taean (blue) and Dangjin (orange) powerplants. The color solid lines and gray dashed line indicate the best-fit and 1:1 line, respectively. Filled and open symbols represent data points which are used in SO_2 estimation or not.

Table 4
Overall comparison of total emission rates of CO_2 (ton h^{-1}) for Taean and Dangjin powerplant implemented by the mass balance and Gaussian footprint methods. The uncertainty associated with each estimate is indicated by the ± symbol, reflecting the quantified uncertainty bounds. EDGAR 2022 and ODIAC 2022 emission inventory for each location are the weight averaged CO_2 emission rates based on the corresponding month of airborne measurement.

Location	Spiral	Mass balance	Gaussian footprint	Ensemble	EDGAR 2022[a]	ODIAC 2022[b]
Taean	S1T	538 ± 1834	2717 ± 297	1628 ± 1706		
	S2T	1617 ± 943	1494 ± 248	1555 ± 692		
	S3T	584 ± 848	861 ± 187	723 ± 629		
	S4T	195 ± 770	660 ± 142	428 ± 601		
	S5T	4566 ± 972	3416 ± 300	3991 ± 921		
	S6T	2860 ± 722	3518 ± 292	3189 ± 641		
	S7T	2113 ± 762	2083 ± 323	2098 ± 585		
	S8T	2775 ± 945	2853 ± 308	2814 ± 704		
	Mean	1906 ± 974	2200 ± 262	2053 ± 585	3467 ± 246	1884 ± 134
Dangjin	S1D	1629 ± 575	2111 ± 261	1870 ± 508		
	S2D	1389 ± 1325	1788 ± 251	1589 ± 974		
	S3D	535 ± 715	820 ± 205	678 ± 545		
	S4D	823 ± 692	1615 ± 247	1219 ± 653		
	S5D	1193 ± 883	1466 ± 432	1329 ± 708		
	S6D	4007 ± 1295	3253 ± 276	3630 ± 1009		
	S7D	1690 ± 1652	2207 ± 272	1949 ± 1212		
	S8D	3847 ± 1237	2543 ± 275	3195 ± 1108		
	S9D	1400 ± 776	2737 ± 277	2068 ± 887		
	S10D	1237 ± 669	1531 ± 241	1384 ± 524		
	Mean	1775 ± 982	2007 ± 274	1845 ± 625	3248 ± 231	2573 ± 183

[a] EDGAR uncertainty: 7.1 % (Oda and Maksyutov, 2011; Solazzo et al., 2021).
[b] ODIAC uncertainty: 7.1 % (Oda and Maksyutov, 2011; Solazzo et al., 2021).

3.4. Comparison of emission rates from the ensemble method and bottom-up emission inventories

Fig. 6a and b presents a comparison of estimated SO_2 emission rates from the ensemble methods for the Taean and Dangjin power plants with real-time CleanSYS observations for 2022 (7 cases) and 2023 (3 cases) with notable variability. The estimated SO_2 emission rates from the ensemble method were generally lower than the CleanSYS observations with absolute discrepancies of 3–29 % for Taean and 17–36 % for Dangjin as discussed in Section 3.2. With respect to the variation in emission rates, the difference from the CleanSYS values at Taean in the 2022 cases was greater by approximately 24 % than that in the 2023 cases, which was similar to results of the ensemble method (29 %). For Dangjin, the underestimation of emission rates was relatively pronounced with differences not only from the CleanSYS observations (35 %) but also from results of the ensemble method (47 %) compared with the values in the 2023 cases. Notably, the estimated SO_2 emission rates obtained with the ensemble method accurately captured the emission pattern from the CleanSYS observations despite the Gaussian footprint model using the constant CAPSS 2021 emission inventory as a priori information.

The estimated CO_2 emission rates from the ensemble method in 2022 (9 cases) and 2023 (9 cases) were compared with values in the EDGAR and ODIAC bottom-up inventories (Fig. 6c and d). In contrast to SO_2 emission rates, the estimated CO_2 emission rates increased from 1665 to 2700 ton h^{-1} for Taean (62 %) and from 1337 to 2445 ton h^{-1} for Dangjin (83 %) during the same periods. The decreasing emission rates of SO_2 were also confirmed by CleanSYS when the data points were extended to match the CO_2 cases (18 cases), and this shows a reduction from 409 kg h^{-1} to 356 kg h^{-1} for Taean (18 %) and from 328 kg h^{-1} to 208 kg h^{-1} for Dangjin (37 %). These increases in CO_2 were relatively higher than those reported in a previous study, which reported an increase of 42–55 % between 2019 and 2021 at the same two power plants under the stable operational load of the power plants, even at times with decreasing SO_2 emission rates (Wong et al., 2024a). This contrasting trend between CO_2 and SO_2 emission rates might reflect additional influences underlying operational factors and not an influence of the pandemic period.

The overestimation of CO_2 emission rates in EDGAR was more pronounced in the 2022 cases at both Taean and Dangjin with values twice as high as those estimated with the ensemble method. The ODIAC emission rate at Taean in the 2022 cases was close to our estimated CO_2 emission rate of 12 %, whereas the ODIAC was 43 % lower in the 2023 cases. The largest overestimation of ODIAC was observed in Dangjin in 2022 at 48 %, which was close to that of EDGAR. It should be noted that the key insight from comparing CO_2 emission rates between bottom-up emission inventories is that results align closely with ODIAC values despite the use of EDGAR data as a priori information in the Gaussian footprint method.

To explain the difference in SO_2 and CO_2 emission rates between the 2022 and 2023 cases at the Taean and Dangjin power plants, operational factors, such as differences in monthly electricity production, and site-specific factors must be considered. When considering only months for which estimations were conducted, the weighted monthly average electricity production in 2022 (October and November) and 2023 (May, October, and November) did not show significant differences. The Taean power plant generated 2088 GWh of electricity in 2023, which slightly decreased by approximately 1 % compared to 2116 GWh in 2022. Similarly, electricity production in Dangjin decreased by approximately 4 % from 2159 GWh in 2022 to 2069 GWh in 2023 (KEPCO, 2022, 2023). Although the decreasing pattern in electricity production from the relevant months of 2022 to 2023 coincided with changes in the SO_2 emission rates, these small differences in electricity production at both power plants were negligible in terms of explaining reductions in SO_2 emission rates. The decreased SO_2 emission rates might be influenced by the use of air pollution control devices, such as flue gas desulfurization (FGD) technology, to capture sulfur emissions (Park et al., 2019) and/or the low sulfur content of coal (Yu et al., 2021).

In contrast, the increasing CO_2 emission rates with constant electricity production might be explained by FGD. The desulfurization process might also contribute to the decrease in SO_2 rates (Van Ewijk and McDowall, 2020; Zhao et al., 2010) and the increase in CO_2 emission rates through the wet limestone-gypsum FGD process. During this process, SO_2 from flue gas dissolves in water to form sulfurous acid (H_2SO_3), which subsequently reacts with limestone ($CaCO_3$) in the reaction tank. The primary chemical reaction is as follows:

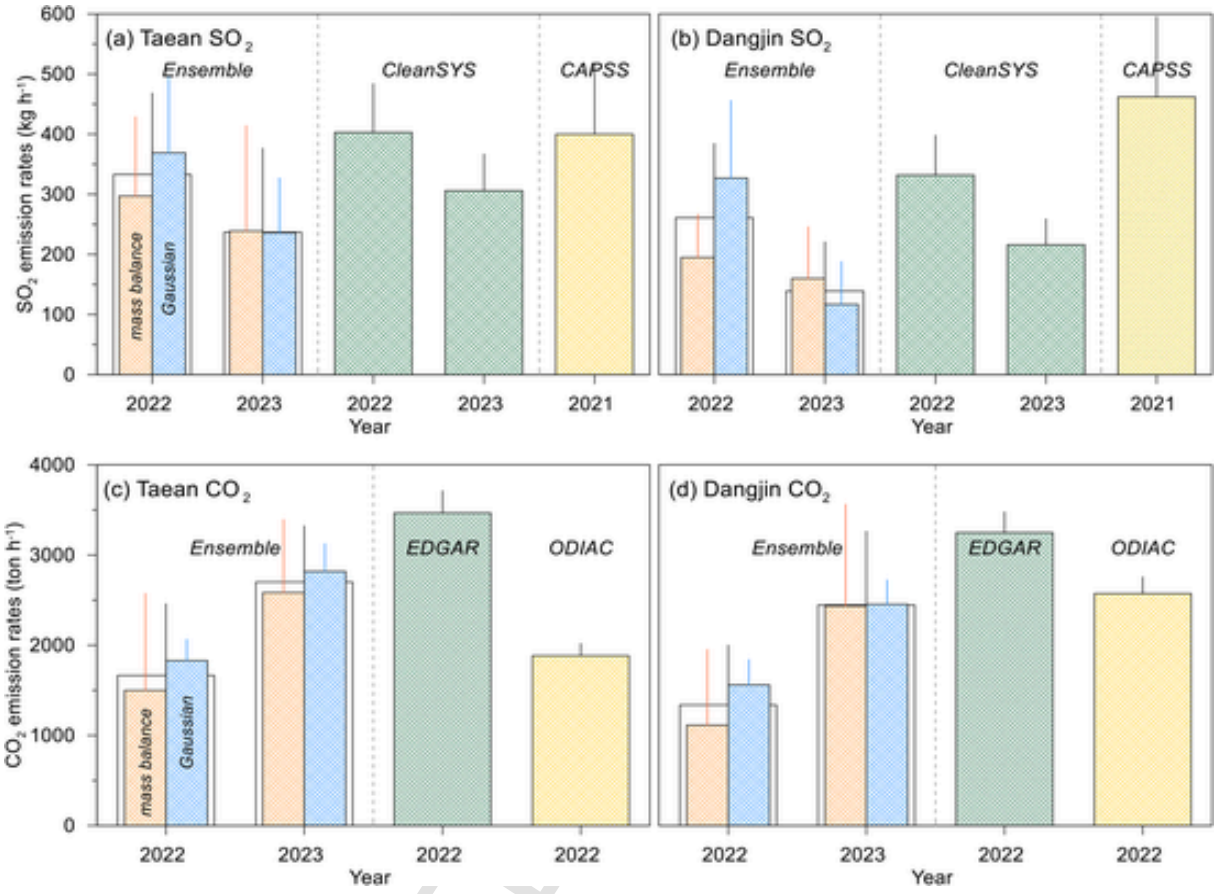

Fig. 6. Comparison of the estimated SO_2 (a and b) and CO2 (c and d) emission rates from our ensemble model with bottom-up emission inventories (EDGARv8.0 and ODIAC) for Taean (left panel) and Dangjin (right panel) powerplants in 2022 and 2023. EDGAR and ODIAC are weight averaged CO_2 emission rates based on the corresponding month of airborne measurement.

$$CaCO_3\,(s) + H_2SO_3\,(aq) \rightarrow CaSO_3\,(s) + CO_2\,(g) + H_2O\,(l)$$

Next, $CaCO_3$ neutralizes sulfurous acid and produces calcium sulfite ($CaSO_3$), water, and CO_2 as a byproduct. However, this mechanism cannot fully explain the observed changes in emission rates at the power plants in this study because there are other contributing factors, such as the usage of carbon-intensive fuel sources (Grant et al., 2021) and/or more intensive operation (Akpan and Fuls, 2021) during research flight periods than at other times, which result in higher estimated CO_2 emissions.

The difference between ODIAC and EDGAR 2022 values and our ensemble estimates can be explained by their spatial resolutions, as both ODIAC and EDGAR provide monthly emission values for short-term comparisons at a high resolution. However, ODIAC has a much finer spatial resolution (1 km by 1 km), requiring summation over several grid cells to match coarser spatial coverage of EDGAR at 0.1° by 0.1° (~11 km by ~11 km). For these reasons, it is difficult to extract solely localized, short-term emissions for the Taean and Dangjin power plants. The coarse resolution of EDGAR leads to significant spatial uncertainties and reduces the accuracy of representing specific emission sources (Ahn et al., 2023; Puliafito et al., 2017). Therefore, the lower emission rates from the top-down approach than from EDGAR are likely a result of its broader spatial resolution, although we accounted for only power plants in our approach.

4. Conclusions

Eighteen representative spiral flights around the Taean and Dangjin power plants were selected for the quantification of SO_2 and CO_2 emission rates via two top-down methodologies: the mass balance method and Gaussian footprint approach. By comparing the curtain plots from the mass balance approach and the footprint results from the Gaussian method, several important conditions can be summarized to accurately quantify emission rates as follows: research should focus on fixed emission sources with (1) a small radius, (2) lower than the PBL height, (3) a fine vertical resolution, and (4) unstable atmospheric stability.

To verify the accuracy of our estimation methods, we validated estimates of the SO_2 emission rate from all selected spirals. Although the R values between the mass balance and Gaussian footprint methods were comparable at >0.70 at the two sites, the mass balance method resulted in a lower SO_2 estimate with relatively high uncertainty, indicating that the Gaussian footprint approach performed more stably. This might be attributed to the choice of extrapolation methods for extending the concentration at the lowest altitude of airborne data to the ground-level concentration. Despite these limitations of the mass balance approach, its variation seems to be much narrower than that of the Gaussian method, which is sensitive under stable conditions at high wind speeds. Thus, this result suggests that averaging emission rates from two approaches (the ensemble method) can provide reasonable estimated SO_2 emission rates because the R (>0.78) and slope of the best-fit line (>0.67) with the CleanSYS data were improved, especially for Dangjin. This finding indicates that the ensemble method is less sensi-

tive to meteorological conditions, making it a reliable approach when atypical conditions are dominant.

By applying the same parameters that produced reliable SO_2 emission rates, we estimated the CO_2 emissions during the same periods extending to the whole dataset. The R value between the results of the mass balance and Gaussian footprint methods was high, at >0.78 at both Taean and Dangjin, along with a similar slope for the best fit lines (~0.48) and high intercepts for ~50 % of the emission rates, indicating that the mass balance method might yield overestimates at low emission rates, and vice versa. The difference between the two methods decreased as the number of available data points increased; thus, both methods generally produced consistent emission estimates, demonstrating their robustness by compensating for their inherent limitations.

On the basis of our ensemble method, the variations in estimated SO_2 and CO_2 emission rates were investigated at the Taean and Dangjin power plants for the 2022 and 2023 cases. The difference in estimated SO_2 emission rates between the relevant months of 2022 and 2023 was coincident with that from the CleanSYS values not only in pattern but also in the magnitude of decrease (38 % for the ensemble method results and 30 % for the CleanSYS values for both power plants). Notably, SO_2 emission rates estimated with the ensemble method accurately capture the emission pattern from the CleanSYS values despite the Gaussian footprint method using the constant CAPSS 2021 emission inventory as a priori information. In contrast to that in SO_2 emission rates, the variation in estimated CO_2 emission rates increased at both Taean (~62 %) and Dangjin (~83 %) during the same periods. CO_2 emission rates in EDGAR were overestimated at both Taean and Dangjin, especially in the 2022 cases, but the ODIAC emission rates were relatively close to our estimated CO_2 emission rates despite the use of monthly EDGAR emission rates as a prior information in the Gaussian footprint approach. Given that the monthly electricity production in the 2022 and 2023 cases did not significantly differ, the decreased SO_2 emission rates might be influenced by the use of air pollution control devices (e.g., flue gas desulfurization technology) and/or the low sulfur content of coal. However, the increasing CO_2 emission rates might be explained by the usage of carbon-intensive fuel sources and/or power plant activity changes during certain periods.

In this study, a reliable ensemble method was developed by combining mass balance and Gaussian footprint approaches to estimate SO_2 and CO_2 emission rates from two large point sources by compensating for the limitations of each model under specific environmental and measurement conditions observed in eighteen selected spirals. These findings emphasize the potential of top-down approaches to improve emission estimates, particularly for large, stationary sources where real-time monitoring systems are limited or unavailable. While the ensemble method demonstrated robust performance under the optimized conditions, its broader applicability to other emission sources or environments should be explored in future research. Therefore, we suggest that this approach can serve as a complementary tool for emission monitoring, especially when used alongside other established bottom-up and top-down methodologies.

CRediT authorship contribution statement

Jeonghwan Kim: Writing – original draft, Visualization, Investigation, Formal analysis, Data curation. **Gangwoong Lee:** Software, Methodology, Conceptualization. **Jongbyeok Jun:** Investigation. **Beum-Keun Seo:** Writing – review & editing, Methodology, Data curation. **Yongjoo Choi:** Writing – review & editing, Writing – original draft, Supervision, Methodology, Conceptualization.

Declaration of competing interest

The authors declare that they have no known competing financial interests or personal relationships that could have appeared to influence the work reported in this paper.

Acknowledgments

This study was supported by the FRIEND (Fine Particle Research Initiative in East Asia Considering National Differences) project through the National Research Foundation of Korea (NRF) funded by the Ministry of Science and ICT, South Korea (Grant No. 2023M3G1A109066421) and by the Hankuk University of Foreign Studies Research Fund of 2024.

Data availability

Data will be made available on request.

Appendix A. Supplementary data

Supplementary data to this article can be found online at https://doi.org/10.1016/j.scitotenv.2025.179430.

References

Ahn, D., Goldberg, D., Coombes, T., Kleiman, G., Anenberg, S., 2023. CO2 emissions from C40 cities: citywide emission inventories and comparisons with global gridded emission datasets. Environ. Res. Lett. 18, 034032.

Ahn, D.Y., Hansford, J.R., Howe, S.T., Ren, X.R., Salawitch, R.J., Zeng, N., Cohen, M.D., Stunder, B., Salmon, O.E., Shepson, P.B., Gurney, K.R., Oda, T., Lopez-Coto, I., Whetstone, J., Dickerson, R.R., 2020. Fluxes of Atmospheric Greenhouse-Gases in Maryland (FLAGG-MD): Emissions of Carbon Dioxide in the Baltimore, MD-Washington, D.C. Area. Journal of Geophysical Research: Atmospheres 125, e2019JD032004. https://doi.org/10.1029/2019JD032004.

Akpan, P.U., Fuls, W.F., 2021. Cycling of coal fired power plants: a generic CO2 emissions factor model for predicting CO2 emissions. Energy 214, 119026.

Bergamaschi, P., Krol, M., Meirink, J.F., Dentener, F., Segers, A., Van Aardenne, J., Monni, S., Vermeulen, A.T., Schmidt, M., Ramonet, M., Yver, C., Meinhardt, F., Nisbet, E.G., Fisher, R.E., O'Doherty, S., Dlugokencky, E.J., 2010. Inverse modeling of European CH4 emissions 2001–2006. Journal of Geophysical Research: Atmospheres 115, 22309. https://doi.org/10.1029/2010JD014180.

Briggs, G.A., 1969. Plume Rise: A Critical Survey.

Brioude, J., Kim, S.W., Angevine, W.M., Frost, G.J., Lee, S.H., McKeen, S.A., et al., 2011. Top-down estimate of anthropogenic emission inventories and their interannual variability in Houston using a mesoscale inverse modeling technique. J. Geophys. Res. Atmos. 116, 20305.

Brioude, J., Angevine, W.M., Ahmadov, R., Kim, S.W., Evan, S., McKeen, S.A., et al., 2013. Top-down estimate of surface flux in the Los Angeles Basin using a mesoscale inverse modeling technique: assessing anthropogenic emissions of CO, NOx and CO2 and their impacts. Atmos. Chem. Phys. 13, 3661–3677.

Cambaliza, M.O.L., Shepson, P.B., Caulton, D.R., Stirm, B., Samarov, D., Gurney, K.R., et al., 2014. Assessment of uncertainties of an aircraft-based mass balance approach for quantifying urban greenhouse gas emissions. Atmos. Chem. Phys. 14, 9029–9050.

Cape, J.N., Fowler, D., Davison, A., 2003. Ecological effects of sulfur dioxide, fluorides, and minor air pollutants: recent trends and research needs. Environ. Int. 29, 201–211.

Carn, S.A., Krueger, A.J., Krotkov, N.A., Yang, K., Levelt, P.F., 2007. Sulfur dioxide emissions from Peruvian copper smelters detected by the Ozone Monitoring Instrument. Geophys. Res. Lett. 34.

Cassia, R., Nocioni, M., Correa-Aragunde, N., Lamattina, L., 2018. Climate change and the impact of greenhouse gasses: CO2 and NO, friends and foes of plant oxidative stress. Front. Plant Sci. 9, 331669.

Chang, L.S., Kim, D., Hong, H., Kim, D.R., Yu, J.A., Lee, K., et al., 2022. Evaluation of correlated Pandora column NO2and in situ surface NO2measurements during GMAP campaign. Atmos. Chem. Phys. 22, 10703–10720.

Choi, Sw, Kim, T., Hk, Lee, Hc, Kim, Han, J., Kb, Lee, et al., 2020. Analysis of the National Air Pollutant Emission Inventory (CAPSS 2016) and the major cause of change in Republic of Korea. Asian J. Atmos. Environ. 14, 422–445.

Crippa, M., Guizzardi, D., Solazzo, E., Muntean, M., Schaaf, E., Monforti-Ferrario, F., et al., 2023. GHG Emissions of All World Countries. Publications Office of the European Union.

Davis, Z.Y.W., Baray, S., McLinden, C.A., Khanbabakhani, A., Fujs, W., Csukat, C., et al., 2019. Estimation of NOx and SO2 emissions from Sarnia, Ontario, using a mobile MAX-DOAS (Multi-AXis Differential Optical Absorption Spectroscopy) and a NOx analyzer. Atmos. Chem. Phys. 19, 13871–13889.

Duncan, B.N., Prados, A.I., Lamsal, L.N., Liu, Y., Streets, D.G., Gupta, P., et al., 2014. Satellite data of atmospheric pollution for U.S. air quality applications: examples of applications, summary of data end-user resources, answers to FAQs, and common

mistakes to avoid. Atmos. Environ. 94, 647–662.
Elguindi, N., Granier, C., Stavrakou, T., Darras, S., Bauwens, M., Cao, H., et al., 2020. Intercomparison of magnitudes and trends in anthropogenic surface emissions from bottom-up inventories, top-down estimates, and emission scenarios. Earth's Future 8, e2020EF001520-e2020EF001520.
Fiehn, A., Kostinek, J., Eckl, M., Klausner, T., Galkowski, M., Chen, J., et al., 2020. Estimating CH4, CO2 and CO emissions from coal mining and industrial activities in the Upper Silesian Coal Basin using an aircraft-based mass balance approach. Atmos. Chem. Phys. 20, 12675–12695.
Fried, A., Walega, J., Weibring, P., Richter, D., Simpson, I.J., Blake, D.R., et al., 2020. Airborne formaldehyde and volatile organic compound measurements over the Daesan petrochemical complex on Korea's northwest coast during the Korea-United States Air Quality study Estimation of emission fluxes and effects on air quality. Elementa: Sci. Anthropocene 8.
Frins, E., Ibrahim, O., Casaballe, N., Osorio, M., Arismendi, F., Wagner, T., et al., 2011. Ground based measurements of SO2 and NO2 emissions from the oil refinery "la Teja" in Montevideo city. J. Phys. Conf. Ser. 274, 12083.
Geddes, J.A., Wang, B., Li, D., 2021. Ozone and nitrogen dioxide pollution in a coastal urban environment: the role of sea breezes, and implications of their representation for remote sensing of local air quality. J. Geophys. Res. Atmos. 126, e2021JD035314.
Gordon, M., Li, S.M., Staebler, R., Darlington, A., Hayden, K., O'Brien, J., et al., 2015. Determining air pollutant emission rates based on mass balance using airborne measurement data over the Alberta oil sands operations. Atmos. Meas. Tech. Discuss. 8, 4769–4816.
Grant, D., Zelinka, D., Mitova, S., 2021. Reducing CO2 emissions by targeting the world's hyper-polluting power plants*. Environ. Res. Lett. 16, 94022.
Hajny, K.D., Lyon, D.R., Armstrong, A., Floerchinger, C.R., Jayarathne, T., Kaeser, R., Lavoie, T., Salmon, O.E., Stirm, B.H., Stuff, A.A., Tomlin, J.M., Wulle, B., Lopez-Coto, I., Shepson, P.B., 2023. Assessing the bias and uncertainties in the aircraft mass balance technique for the determination of carbon dioxide emission rates. Elementa 11. https://doi.org/10.1525/ELEMENTA.2022.00135/196735.
Jeon, E.C., Myeong, S., Sa, J.W., Kim, J., Jeong, J.H., 2010. Greenhouse gas emission factor development for coal-fired power plants in Korea. Appl. Energy 87, 205–210.
Kahl, J.D.W., Chapman, H.L., 2018. Atmospheric stability characterization using the Pasquill method: a critical evaluation. Atmos. Environ. 187, 196–209.
KEPCO, 2022. https://home.kepco.co.kr/kepco/KO/ntcob/list.do?pageIndex=2&boardSeq=0&boardCd=BRD_000097&menuCd=FN05030101&parnScrpSeq=0&categoryCdGroup=&regDateGroup1=.
KEPCO, 2023. https://home.kepco.co.kr/kepco/KO/ntcob/list.do?pageIndex=2&boardSeq=0&boardCd=BRD_000097&menuCd=FN05030101&parnScrpSeq=0&categoryCdGroup=&regDateGroup1=.
Kim, J., Jang, Y.-K., 2014. Uncertainty assessment for CAPSS emission inventory by DARS. J. Kor. Soc. Atmos. Environ. 30, 26–36.
Kim, J., Seo, B.-k., Lee, T., Kim, J., Kim, S., Bae, G.-N., et al., 2023. Airborne estimation of SO2 emissions rates from a coal-fired power plant using two top-down methods: a mass balance model and Gaussian footprint approach. Sci. Total Environ. 855, 158826.
Köne, A.I., Büke, T., 2010. Forecasting of CO2 emissions from fuel combustion using trend analysis. Renew. Sust. Energ. Rev. 14, 2906–2915.
Kuhlmann, G., Henne, S., Meijer, Y., Brunner, D., 2021. Quantifying CO2 emissions of power plants with CO2 and NO2 imaging satellites. Front. Remote Sens. 2, 689838.
Kurokawa, J., Ohara, T., Morikawa, T., Hanayama, S., Janssens-Maenhout, G., Fukui, T., et al., 2013. Emissions of air pollutants and greenhouse gases over Asian regions during 2000-2008: Regional Emission inventory in ASia (REAS) version 2. Atmos. Chem. Phys. 13, 11019–11058.
Mao, S., Lang, J., Chen, T., Cheng, S., Hu, F., 2022. Comparative study of source inversion under multiple atmospheric pollutant emission scenarios. Front. Environ. Sci. 10, 857701.
McDuffie, E.E., Smith, S.J., O'Rourke, P., Tibrewal, K., Venkataraman, C., Marais, E.A., et al., 2020. A global anthropogenic emission inventory of atmospheric pollutants from sector- and fuel-specific sources (1970-2017): an application of the Community Emissions Data System (CEDS). Earth System Sci. Data 12, 3413–3442.
McLinden, C.A., Fioletov, V., Boersma, K.F., Krotkov, N., Sioris, C.E., Veefkind, J.P., et al., 2012. Air quality over the Canadian oil sands: a first assessment using satellite observations. Geophys. Res. Lett. 39.
Nassar, R., Mastrogiacomo, J.P., Bateman-Hemphill, W., McCracken, C., MacDonald, C.G., Hill, T., et al., 2021. Advances in quantifying power plant CO2 emissions with OCO-2. Remote Sens. Environ. 264, 112579.
Oda, T., Maksyutov, S., 2011. A very high-resolution (1 km ×1 km) global fossil fuel CO2 emission inventory derived using a point source database and satellite observations of nighttime lights. Atmos. Chem. Phys. 11, 543–556.
Oda, T., Maksyutov, S., 2015. ODIAC Fossil Fuel CO2 Emissions Dataset (Version Name: ODIAC2023). National Institute for Environmental Studies, Center for Global Environmental Research. (accessed: 2024/09/05).
Orellano, P., Reynoso, J., Quaranta, N., 2021. Short-term exposure to sulphur dioxide (SO2) and all-cause and respiratory mortality: a systematic review and meta-analysis. Environ. Int. 150, 106434.
Park, J.H., Ahn, J.W., Kim, K.H., Son, Y.S., 2019. Historic and futuristic review of electron beam technology for the treatment of SO2 and NOx in flue gas. Chem. Eng. J. 355, 351–366.
Park, M., Hu, H., Kim, Y., Fried, A., Simpson, I.J., Jin, H., et al., 2023. Evaluation of the emission inventory for large point emission sources in South Korea by applying measured data from the NASA/NIER KORUS-AQ aircraft field campaign. Elementa 11.
Puliafito, S.E., Allende, D.G., Castesana, P.S., Ruggeri, M.F., 2017. High-resolution atmospheric emission inventory of the argentine energy sector. Comparison with Edgar global emission database. Heliyon 3, e00489.
Qu, Z., Henze, D.K., Worden, H.M., Jiang, Z., Gaubert, B., Theys, N., et al., 2022. Sector-based top-down estimates of NOx, SO2, and CO emissions in East Asia. Geophys. Res. Lett. 49, e2021GL096009.
Sanchez, N.P., Saffari, A., Barczyk, S., Coleman, B.K., Naufal, Z., Rabideau, C., et al., 2019. Results of three years of ambient air monitoring near a petroleum refinery in Richmond, California, USA. Atmosphere 10, 385.
Seibert, P., Frank, A., 2004. Source-receptor matrix calculation with a Lagrangian particle dispersion model in backward mode. Atmos. Chem. Phys. 4, 51–63.
Seo, B.K., Sb, Park, Lee, D., Yu, M., Yu, J., Bae, K.N., et al., 2019. Airborne inlets and instrumentation on aircraft platform for air quality observation. J. Kor. Soc. Atmos. Environ. 35, 815–830.
Solazzo, E., Crippa, M., Guizzardi, D., Muntean, M., Choulga, M., Janssens-Maenhout, G., 2021. Uncertainties in the Emissions Database for Global Atmospheric Research (EDGAR) emission inventory of greenhouse gases. Atmos. Chem. Phys. 21, 5655–5683.
Souri, A.H., Kumar, R., Chong, H., Golbazi, M., Knowland, K.E., Geddes, J., et al., 2023. Decoupling in the vertical shape of HCHO during a sea breeze event: the effect on trace gas satellite retrievals and column-to-surface translation. Atmos. Environ. 309, 119929.
Stohl, A., Seibert, P., Arduini, J., Eckhardt, S., Fraser, P., Greally, B.R., et al., 2009. An analytical inversion method for determining regional and global emissions of greenhouse gases: sensitivity studies and application to halocarbons. Atmos. Chem. Phys. 9, 1597–1620.
Szulejko, J.E., Kumar, P., Deep, A., Kim, K.H., 2017. Global warming projections to 2100 using simple CO2 greenhouse gas modeling and comments on CO2 climate sensitivity factor. Atmos. Pollut. Res. 8, 136–140.
Theys, N., De Smedt, I., Van Gent, J., Danckaert, T., Wang, T., Hendrick, F., et al., 2015. Sulfur dioxide vertical column DOAS retrievals from the Ozone Monitoring Instrument: global observations and comparison to ground-based and satellite data. J. Geophys. Res. Atmos. 120, 2470–2491.
Van Ewijk, S., McDowall, W., 2020. Diffusion of flue gas desulfurization reveals barriers and opportunities for carbon capture and storage. Nat. Commun. 11.
Wong, G., Park, M., Park, J., Ahn, J.Y., Sung, M., Choi, J., et al., 2024a. Investigating the impact of control strategies on the sulfur dioxide emissions of South Korean industrial facilities using an aircraft mass balance approach. Atmos. Environ. 328, 120496.
Wong, G., Wang, H., Park, M., Park, J., Ahn, J.Y., Sung, M., et al., 2024b. Optimizing an airborne mass-balance methodology for accurate emission rate quantification of industrial facilities: a case study of industrial facilities in South Korea. Sci. Total Environ. 912, 169204.
Yu, J.H., Song, J., Lee, D.Y., Yu, M.S., Jung, J.H., Chun, S.N., et al., 2021. Comparison of PMtotal, PM10, PM2.5, NOx, and SO2 emission factors from coal-fired power plants per load change. Asian J. Atmos. Environ. 15, 1–10.
Zhao, Y., Wang, S., Nielsen, C.P., Li, X., Hao, J., 2010. Establishment of a database of emission factors for atmospheric pollutants from Chinese coal-fired power plants. Atmos. Environ. 44, 1515–1523.
Zondlo, M.A., 2021. Unmanned aerial systems for trace gases. Adv. Spectrosc. Monit. Atmos. 321–343.